PARAMETRIC STUDIES OF SHAPE MEMORY ALLOY HYBRID COMPOSITE LAMINATES UNDER LOW-VELOCITY IMPACT

Y.-C. Lin *

School of Defense Science
Chung Cheng Institute of Technology
National Defense University
Taoyuan, Taiwan

Y.-L. Chen

Department of Power Vehicle and Systems Engineering
Chung Cheng Institute of Technology
National Defense University
Taoyuan, Taiwan

H.-W. Chen

Chung San Institute of Sciences and Technology
Taoyuan, Taiwan

ABSTRACT

In the paper, the influence of shape memory alloy (SMA) by varying the parameters such as volume fraction, orientation, and temperature on the hybrid-SMA composite laminate subjected to low-velocity impact is studied. A theoretical model for the composite laminated plate bonded with SMA reinforced layers is presented. The constitutive relation of the SMA layer is obtained by using the method of micromechanics. The governing relations obtained can be used for theoretical predications of thermomechanical properties of SMA plies in this paper. The analytical expressions for the hybrid SMA composite plate are derived based on Tanaka's constitutive equation and linear phase transformation kinetics presented by Liang and Rogers.

The laminated plate theory, first-order shear deformation theory and minimal potential energy principle is utilized to solve the governing equations of the hybrid composite plate and calculate the absorbed energies including tensile, shear and bending.

An orthogonal array and analysis of variance is employed to investigate the influence of the mentioned parameters on the energy absorption of the hybrid laminated plate. The results showed that the effects of the phase transformation temperature are more significant than the effects of the volume fraction and orientation of SMA on structural energy absorption.

Keywords: Shape memory alloy, Composite laminate, Impact, Analysis of variance.

1. INTRODUCTION

Composite materials are known to have a poor resistance to through-the-thickness impact loading. The problem of transverse impact of composite structures represents significant practical and theoretical interest. The need for improved materials with better strength, and lower weight leads to the use of composite materials in the aerospace structures [1,2].

One possible way to increase impact damage resistance of composite structure is by embedding SMA wires or plies into composite structures. Smart materials can present an attractive tool for reducing deflections and stresses in the structures subjected to a low-velocity impact. In particular, shape memory alloys (SMA) can generate significant tensile stresses. The necessary effect can be achieved if SMA fibers are embedded within a composite material resulting in a hybrid smart composite [3,4].

Recently, in order to increase impact resistance, research has focused increasing attention on applications of the smart structure concept for composite structures. The interest on shape memory alloys has been growing over recent decades due to their remarkable properties in developing smart composites that are capable of adapting intelligently to external disturbances. Shape memory alloy has advantages in terms of a high power to volume ratio; they are suitable for impact problems of large deformation. SMA also has the unique capability of changing their physical properties, such as stiffness, damping ratio and viscosity, in response to external stimuli and thus can be considered smart mate-

* Corresponding author (g951701@hotmail.com)

DOI : 10.1017/jmech.2016.24
Copyright © 2016 The Society of Theoretical and Applied Mechanics
https://doi.org/10.1017/jmech.2016.24 Published online by Cambridge University Press

rials. Hence, SMA is suitable for impact problems that accompany large deformations. SMA has two inherent characteristics: One is the shape memory effect (SME) and the other is super-elasticity or pseudo-elasticity [5,6].

Some researchers used experimental data excluding the phase transformation processes for behavior modeling of the SMAs. However, the constitutive mathematical models for description of the phase transformation kinetics have mainly been proposed by Tanaka [5-8], Liang and Rogers [5,7,9], Brinson [8-16]. Some researchers [5,8,12,13] re-investigated the Tanaka, Liang and Rogers, and Brinson models for numerical simulation analyses of the thermal behavior of laminated composites with embedded SMA wires performed to investigate the effect of embedded SMA wires. In order to simulate the thermo-mechanical behavior of SMA wires, the constitutive equation of the SMA wires is formulated by showing the response of the pseudo-elasticity and SME at various temperatures and stress levels. The thermal analyses of the composites with embedded SMA wires show that the temperature can be increased and the deformation can be decreased by using the activation force of embedded SMA wire actuators.

Moreover, many vibration modes including continuous and discrete models is investigated. The discrete model for nonlinear low-velocity impact analysis of two-directionally-graded circular plates under radial preloads is presented by using nonlinear von Karman-type strain-displacement relations. The behavior simulation of plates cannot incorporate effects of the higher vibration modes comparable to fundamental vibration mode of the plate in some cases [17].

Thus, continuous models are considered by some researchers to numerically investigate impact responses of the SMA hybrid composite plates. Using the concept of recovery stresses of SMAs [18] instead of using the constitutive laws, is not enough to investigate influence of the SMAs on the impact responses. In the research, the variations of the volume fraction of the martensite phase of the SMA have not been considered in the employed formulation. In contrast, for example, Meo *et al*. [3] considered super-elastic and hysteretic behaviour of the SMAs through a simple numerical model. The super-elastic effect is due to reversible stress induced transformation from austenite to martensite.

However, for a more efficient application of the SMAs, numerical modeling procedures have to be utilized by Brinson's model and finite element method and using Newmark integration method and Hertz's law. The pseudo-elastic effect of the SMAs on the low-velocity impact responses of a hybrid composite plate is investigated by Wu *et al*. [19] However, the Effects of shape memory alloy thin films embedded in composite plates are investigated using Chang–Chang failure criteria model by Kim *et al*. [20], implementing Lagoudas' model in ABAQUS finite element analysis code. A review of recent SMA research and applications is presented by Mohd *et al*. [21].

Although many studies on the vibration analysis of buckled composite laminates [5,15-17,22-24] or the optimum design of SMA reinforced composite laminates [18] have been published, relatively few works have been devoted to the study of the impact analysis include tensile fracture energy, Shear bending fracture energy and delamination energy in the SMA reinforced composite laminates.

In the present research, the effect of SMA on the impact behavior of cross-ply laminates by varying orientation, volume fraction and temperature is investigated. The impact analysis is performed for composite laminated plates with embedded SMA plies through modifying Tanaka's model. In this regard, the constitutive laws of the SMA, and the strain–displacement relations are considered through a solution scheme that is employed. The governing relationships obtained in this paper can be used for theoretical predications of thermo-mechanical properties of SMA plies. The formulation of the stiffness matrix due to material properties and the temperature-dependent recovery stress stiffness matrix are derived. Parametric studies are performed to investigate the effect of shape memory alloys for improving impact resistance of composite plate in detail. The laminated plate theory, first-order shear deformation theory and minimal potential energy principle are used in the hybrid composite plates. The results showed that SMA fibers is effective in improving impact resistance capacity.

2. CONSTITUTIVE EQUATIONS FOR SMA FIBERS

The SMA material behavior model is complex and non-linear. Over the years, researchers have constructed constitutive models for a SMA by adopting several aspects, such as the elasticity/plasticity theory, the thermal dynamic theory, chemical free energy, crystal phase dynamics, and the energy dissipation theory. Generally, these can be divided into microscale models and macroscale models. Although a microscale model can precisely illustrate the influences produced by the various parameters on a material's mechanical behavior, it is more complex and impractical in engineering applications.

In 1986, Tanaka explored a material dynamic behavior model for a SMA by using the thermal dynamic and phase transformation dynamic theories. Based on energy conservation and the Clausius-Duhem inequality, an exponential model, which the stress, strain, temperature, and material crystal phase fraction were deduced and verified to be a set of state variables, is proposed to illustrate the entire material behavior of the SMA in his study.

Afterward, Liang and Rogers proposed the cosine Martensite transformation dynamic model to substitute for the exponential model of Tanaka. In his study, 1-D constitutive relationship model for a SMA was developed by fitting experimental data. However, compared with other models, it is practical and simple to use in engineering applications.

https://doi.org/10.1017/jmech.2016.24 Published online by Cambridge University Press

In this research, rectangular laminates consisting of weave layers are considered. The Nitinol/epoxy are supposed to be embedded within the different layers of the laminate symmetrically to the smart hybrid composite structure. Therefore, the 1-D constitutive relationship developed by Liang and Rogers is used to derive the mechanical model for the fiber-reinforced composite tube structure incorporated with a SMA in this study.

The constitutive relationship [5] formed by Liang and Rogers is shown as below:

$$\sigma - \sigma_0 = E(\varepsilon - \varepsilon_0) + \theta(T - T_0) + \Omega(\xi - \xi_0) \tag{1}$$

where σ, E, ε, θ, T, Ω, and ξ are the stress, Young's modulus, strain, thermal elasticity tensor, temperature, phase transformation tensor, and Martensite phase fraction ($0 \le \xi \le 1$) of the material, respectively. σ_0, ε_0, T_0, and ξ_0 are the initial conditions of the stress, strain, temperature, and Martensite phase fraction, respectively.

The SME of the SMA results from the transformation of two stable phases. One is the austensite, which is a stable phase at a high temperature, and the other is the martensite, which is a stable phase at a low temperature. The martensite fraction in the alloy is related not only to the temperature and stress, but also to the direction of the phase transformation.

For the martensite to austenite transformation, ξ is given by

$$\xi = \frac{1}{2}\xi_M \left\{\cos\left[a_A(T - A_S) - b_A\sigma\right] + 1\right\} \tag{2}$$

and for the austenite to martensite transformation,

$$\xi = \frac{1}{2}(1 - \xi_A)\cos\left[a_M(T - M_F) - b_M\sigma\right] + \frac{1}{2}(1 + \xi_A) \tag{3}$$

In the above equations, ξ_M and ξ_A represent the martensite phase fractions at the beginning of the phase transformation when the M→A or the A→M transformation starts from a state which has mixed austenite and martensite phases. a_A, a_M, b_A, and b_M are the material constants, which can be defined as follows:

$$a_A = \frac{\pi}{A_F - A_S},\ a_M = \frac{\pi}{M_S - M_F},\ b_A = \frac{a_A}{C_A},\ b_M = \frac{a_M}{C_M} \tag{4}$$

and A_S, A_F, M_S and M_F are the austenite and martensite start and finish temperatures of the SMA under stress free condition, respectively; T is temperature and σ is stress; C_A and C_M are SMA material constants related to stress-induced phase transformation.

In Eqs. (2) and (3), the cosine function is limited in range, [0, π]. Therefore, when the transformation is from Martensite into Austensite, the range of the stress is shown as below:

$$C_A(T - A_f) \le \sigma \le C_A(T - A_S) \tag{5}$$

when the transformation is from Austensite into Martensite, the range of the stress is shown as below:

$$C_M(T - M_S) \le \sigma \le C_M(T - M_f) \tag{6}$$

The change of the Young's modulus in different states of phase transformation should also be considered when constructing a mechanical behavior model for the SMA material. When the SMA is activated by heat, the martensite phase fraction will vary accordingly. Simultaneously, the Young's modulus, E, and the phase transformation coefficient, Ω, will also change. That is to say, when the SMA goes into the phase transformation process, the Young's modulus, E, and the phase transformation tensor, Ω, need to be adjusted according to the phase fraction. The relationship between this adjustment and the phase fraction is shown as follows:

$$E(\xi) = E_A + \xi(E_M - E_A) \tag{7}$$

$$\Omega = -\varepsilon_L \cdot E \tag{8}$$

where E_M and E_A are the Young's modulus value for the SMA of 100% martensite and austenite, respectively. ε_L is the maximum recovery strain of the SMA.

In order to solve the non-linear constitutive relationship of the material mentioned above, Eqs. (2) and (3) are differentiated in the first step, and the differential phase fraction, $d\xi$, is substituted by the differential activation temperature, dT, and the differential stress, $d\sigma$. In the solution process, recursive computation is carried out from the beginning point of the crystal phase transformation until the stress converges completely. The Young's modulus and stress at the beginning point of the phase transformation can therefore be determined. Furthermore, the Young's modulus and stress at the next crystal phase transformation point can also be obtained by following this procedure. A solution flowchart for the course of the overall crystal phase transformation is shown in Fig. 1 [5]. The solved stress is the recovery stress induced by activating the SMA.

3. FORMULATION OF COMPOSITE LAMINATED PLATES

Consider a rectangular composite laminated plate with length a, width a, and thickness h as shown in Fig. 2. The displacement field may be expressed as

$$u(x, y, z) = u_0(x, y) - zw_{0,x} \tag{9}$$

$$v(x, y, z) = v_0(x, y) - zw_{0,y} \tag{10}$$

$$w(x, y, z) = w_0(x, y) \tag{11}$$

where u_0 and v_0 are the mid-plane in-plane displacement components of the plate. w_0 is the out-of-plane displacement component of the plate. The kinematic relation can be determined as

https://doi.org/10.1017/jmech.2016.24 Published online by Cambridge University Press

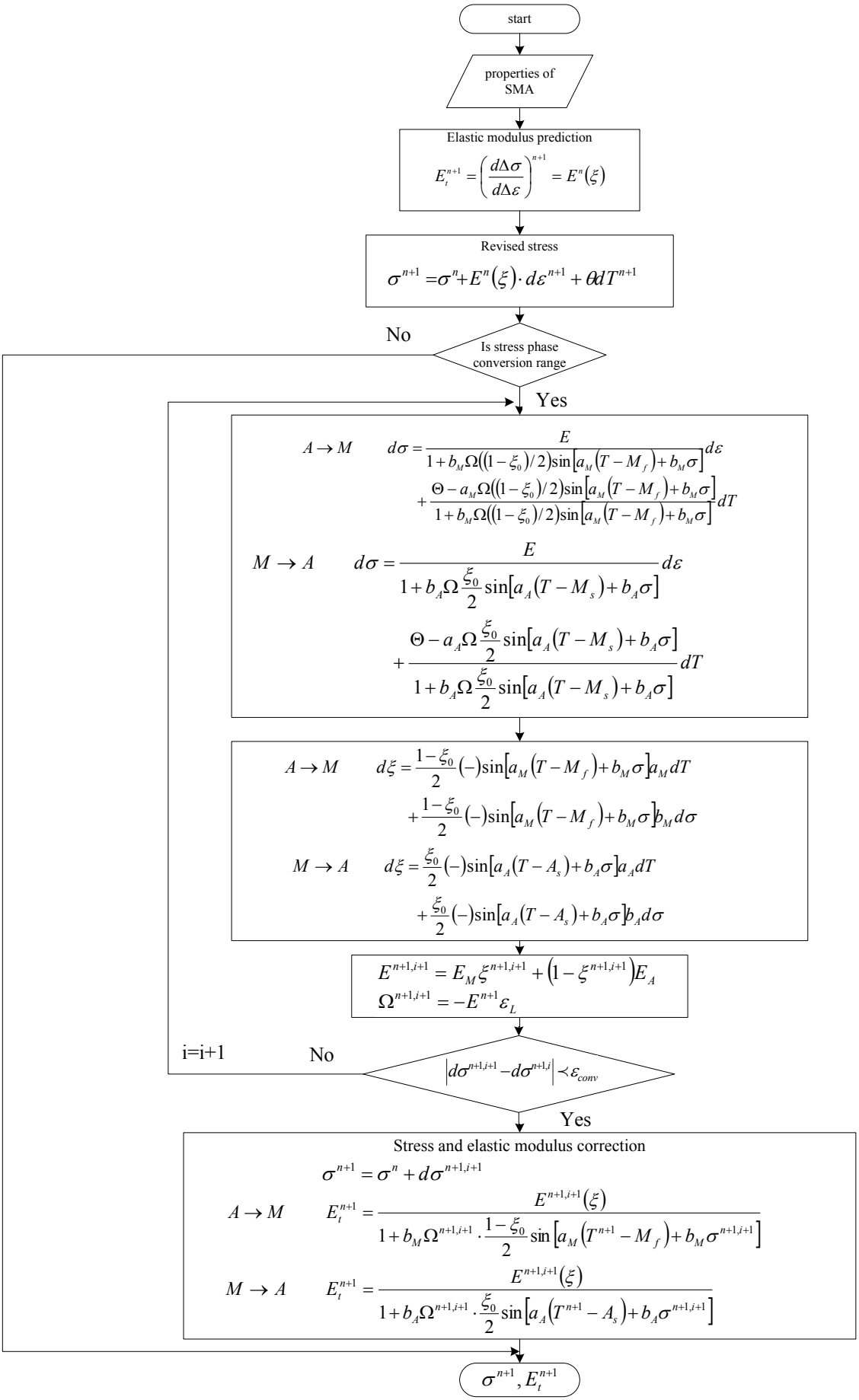


Fig. 1 Solution flowchart of the SMA constitutive equations [5].

https://doi.org/10.1017/jmech.2016.24 Published online by Cambridge University Press

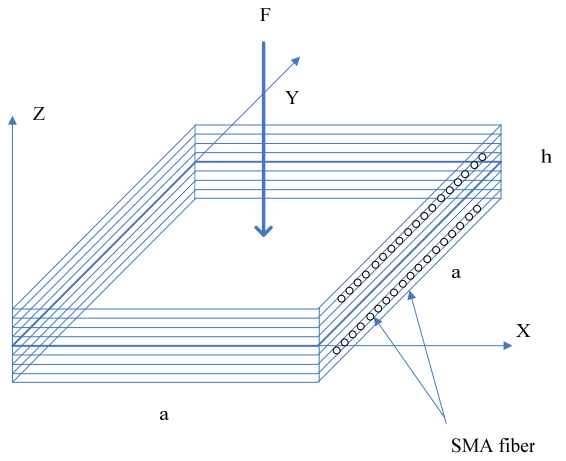


Fig. 2 Configuration and coordinate system of the SMA hybrid composite plate.

$$\begin{Bmatrix}\varepsilon_x\\ \varepsilon_y\\ \gamma_{xy}\end{Bmatrix}=\begin{Bmatrix}u_{0,x}\\ v_{0,y}\\ u_{0,y}+v_{0,x}\end{Bmatrix}-z\begin{Bmatrix}w_{0,xx}\\ w_{0,yy}\\ 2w_{0,xy}\end{Bmatrix}=\{\varepsilon^0\}-z\{k\} \tag{12}$$

where $\{\varepsilon^0\}$ and $\{k\}$ are the mid-plane strain and plate curvature, respectively.

The SMA embedded composite plates are made of Kevlar/epoxy lamina and SMA composite lamina. The Kevlar/epoxy plys are stacked symmetrically on the top and bottom of the Nitinol/epoxy ply to make the SMA reinforced lamina. The SMA hybrid composite plates are made of composite lamina and SMA lamina. The composite lamina is Kevlar/epoxy and SMA lamina is Nitinol/epoxy.

The variable SMA fiber spacing, the elastic moduli E_1, E_2, v_{12} and G_{12} for the Nitinol/epoxy ply are also functions of $V_f^{sma}(\xi)$.

According to the micro-mechanical homogenization techniques, effective material properties of the laminate may be related to those of the fiber and matrix through the following relations:

In this study, the formulas used for the calculation of these effective engineering constants are based on the rule of mixture [4,6,24].

$$E_1(\xi)=E_fV_f^{sma}(\xi)+E_mV_m \tag{13}$$

$$E_2(\xi)=\frac{E_fE_m}{E_fV_m+E_mV_f^{sma}(\xi)} \tag{14}$$

$$v_{12}(\xi)=v_fV_f^{sma}(\xi)+v_mV_m \tag{15}$$

$$G_{12}(\xi)=\frac{G_fG_m}{G_fV_m+G_mV_f^{sma}(\xi)} \tag{16}$$

$$\rho(\xi)=\rho_fV_f^{sma}(\xi)+\rho_mV_m \tag{17}$$

where V_f^{SMA} and V_m are volume fractions of the Nitinol fiber and matrix, respectively, and the subscripts f and m denote the Nitinol fiber and matrix, respectively. The stress-strain relation for the orthotropic SMA composite lamina with variable SMA fiber spacing can be expressed as

$$\begin{Bmatrix}\sigma_1\\ \sigma_2\\ \tau_{12}\end{Bmatrix}=\begin{bmatrix}Q_{11}(\xi) & Q_{12}(\xi) & 0\\ Q_{11}(\xi) & Q_{22}(\xi) & 0\\ 0 & 0 & Q_{66}(\xi)\end{bmatrix}\begin{Bmatrix}\varepsilon_1\\ \varepsilon_2\\ \gamma_{12}\end{Bmatrix}+V_f^{SMA}\begin{Bmatrix}\sigma_1^r\\ 0\\ 0\end{Bmatrix} \tag{18}$$

where

$$Q_{11}(\xi)=\frac{E_1(\xi)}{1-v_{12}(\xi)\,v_{21}(\xi)}$$

$$Q_{12}(\xi)=\frac{v_{21}(\xi)E_1(\xi)}{1-v_{12}(\xi)\,v_{21}(\xi)}$$

$$Q_{22}(\xi)=\frac{E_2(\xi)}{1-v_{12}(\xi)\,v_{21}(\xi)}$$

$$Q_{66}(\xi)=G_{12}(\xi)$$

σ_1^r denotes the temperature-dependent SMA recovery stress in the SMA fiber direction.

If the fiber's orientation with the geometric x axis is denoted by θ, the stress-strain relation is transferred to the geometric coordinates as

$$\begin{Bmatrix}\sigma_1\\ \sigma_2\\ \tau_{12}\end{Bmatrix}=\begin{bmatrix}\overline{Q_{11}}(\xi) & \overline{Q_{12}}(\xi) & \overline{Q_{16}}(\xi)\\ \overline{Q_{12}}(\xi) & \overline{Q_{22}}(\xi) & \overline{Q_{26}}(\xi)\\ \overline{Q_{16}}(\xi) & \overline{Q_{26}}(\xi) & \overline{Q_{66}}(\xi)\end{bmatrix}\begin{Bmatrix}\varepsilon_1\\ \varepsilon_2\\ \gamma_{12}\end{Bmatrix}+V_f^{SMA}\begin{Bmatrix}\sigma_x^r\\ \sigma_y^r\\ \sigma_{xy}^r\end{Bmatrix} \tag{19}$$

where

$$\overline{Q}_{11}=Q_{11}\cos^4\theta+2(Q_{12}+2Q_{66})\sin^2\theta\cos^2\theta+Q_{22}\sin^4\theta$$

$$\overline{Q}_{12}=(Q_{11}+Q_{22}-4Q_{66})\sin^2\theta\cos^2\theta+Q_{12}(\sin^4\theta+\cos^4\theta)$$

$$\overline{Q}_{22}=Q_{11}\sin^4\theta+2(Q_{12}+2Q_{66})\sin^2\theta\cos^2\theta+Q_{22}\sin^4\theta$$

$$\overline{Q}_{16}=(Q_{11}-Q_{12}-2Q_{66})\sin\theta\cos^3\theta+(Q_{12}-Q_{22}+2Q_{66})\sin^3\theta\cos\theta$$

$$\overline{Q}_{26}=(Q_{11}-Q_{12}-2Q_{66})\sin^3\theta\cos\theta+(Q_{12}-Q_{22}+2Q_{66})\sin\theta\cos^3\theta$$

$$\overline{Q}_{66}=(Q_{11}+Q_{22}-2Q_{12}-2Q_{66})\sin^2\theta\cos^2\theta+Q_{66}(\sin^4\theta+\cos^4\theta)$$

It is constructive to calculate and compare the energy absorbed by each mechanism during panel perforation. Doing so provides insight into designing composites for greater perforation resistance or energy absorption. Calculations of the energy absorbed by tensile fracture energy and shear bending fracture energy are given below.

https://doi.org/10.1017/jmech.2016.24 Published online by Cambridge University Press

4. FRACTURE ENERGIES OF LAMINATED STRUCTURE UNDER IMPACT

In this study, the fracture energy of laminated structure under impact is divided into two types: tensile energy and shear bending energy. Ballistic Performance Indicator (B.P.I.), the total energy absorbing per areal density [25], is introduced in the analyses.

4.1 Tensile Fracture Energy

Finite deflection (membrane) theory and the principle of minimum potential energy are used to estimate the energy absorbed in membrane stretching [4,6,26,27]. The membrane energy is given by

$$U_T = \frac{1}{2}\int_0^{a/2}\int_0^{a/2}\left\{A_{11}\left(\frac{\partial w}{\partial x}\right)^4 + A_{22}\left(\frac{\partial w}{\partial y}\right)^4 + (2A_{12}+4A_{66})\left(\frac{\partial w}{\partial x}\right)^2\left(\frac{\partial w}{\partial y}\right)^2\right\}dxdy \tag{20}$$

where A_{ij} is the tensile (membrane) stiffness.

4.2 Shear Bending Fracture Energy

The principle of minimum potential energy is again used to estimate the global panel response. The perforation behavior of fiber laminated composite plates and referenced first-order shear deformation theory combined with the shear effect to produce the shear bending energy formula, as shown below [4,6,26,27].

$$U_{bs} = 2\int_0^{a/2}\int_0^{a/2}\left\{D_{11}\left(\frac{\partial\bar{\alpha}}{\partial x}\right)^2 + 2D_{12}\left(\frac{\partial\bar{\alpha}}{\partial x}\right)\left(\frac{\partial\bar{\beta}}{\partial y}\right) + D_{22}\left(\frac{\partial\bar{\beta}}{\partial y}\right)^2 + A_{55}\left[\bar{\alpha}^2 + 2\bar{\alpha}\frac{\partial w}{\partial x} + \left(\frac{\partial w}{\partial x}\right)^2\right] + A_{44}\left[\bar{\beta}^2 + 2\bar{\beta}\frac{\partial w}{\partial y} + \left(\frac{\partial w}{\partial y}\right)^2\right] + 2D_{66}\left[\left(\frac{\partial\bar{\alpha}}{\partial y}\right)^2 + 2\left(\frac{\partial\bar{\alpha}}{\partial y}\right)\left(\frac{\partial\bar{\beta}}{\partial x}\right) + \left(\frac{\partial\bar{\beta}}{\partial x}\right)^2\right]\right\}dxdy \tag{21}$$

where w is the transverse plate deflection, $\bar{\alpha}$ and $\bar{\beta}$ are rotations with respect to the x and y-axes, respectively, D_{ij} is the bending stiffness matrix and $A_{44} = hG_{23}$ and $A_{55} = hG_{13}$ are the shear rigidities.

5. ANALYSIS PROCEDURE

5.1 Model Description

The 16-plies $\left[(0/90)^{kevlar}/(0/90)^{SMA}/(0/90)_2^{kevlar}\right]_s$ laminate with clamped edges is investigated. For this model, the impact is a diameter of 9mm. In this example, the properties of kevlar/epoxy are shown in Table 1. The dimensions of the plate are 150mm × 150mm. The properties of SMA and epoxy are shown in Tables 2 and 3, respectively.

Table 1 Material properties of Kevlar/epoxy.

Longitudinal tensile modulus	$E_{11} = E_{22} = 18.5$GPa
Transverse tensile modulus	$E_{33} = 6.0$GPa
Shear modulus	$G_{12} = 0.77$GPa $G_{13} = G_{23} = 2.715$GPa
Poisson's ratio	$v_{12} = 0.25$ $v_{13} = v_{23} = 0.33$
Density	1230Kg/m^3

Table 2 Material properties of SMA.

Young's modulus	$D_A = 67.0$GPa $D_M = 26.3$GPa
Thermo-elastic tensor	$\Theta = 0.55$MPa
Recovery strain limit	$\varepsilon_L = 0.067$
Four phase transformation temperature	$M_f = 9$°C, $M_s = 18.4$°C $A_s = 34.5$°C, $A_f = 49$°C
Transition stiffness (stress/temperature)	$C_A = 8$MPa/°C $C_M = 13.8$MPa/°C
Density	6500.00Kg/m^3

Table 3 Material properties of epoxy.

Young's modulus	$E^m = 4.6$GPa
Poisson's ratio	$v^m = 0.366$

5.2 Analysis Settings and Layout

The tests are conducted as per the standard orthogonal array. To select an appropriate orthogonal array for analysis, the total degrees of freedom need to be computed. The selection of the orthogonal array is based on the condition that the degrees of freedom for the orthogonal array should be greater than or equal to sum of those parameters. The degrees of freedom are defined as the number of comparisons between process parameters that need to be made to determine which level is better and specifically how much better it is.

In the present investigation, there are 18 degrees owing to the three impact parameters and the interactions between parameters. Once the degrees of freedom required are known, the next step is to select an appropriate orthogonal array to fit the specific task. In this study, an L_{27} orthogonal array is chosen. A total of 27 runs (3^3) must be conducted in conventional full factorial experiment design, based on combination of three control factors, each with three levels as indicated in Table 4.

The influence of each control parameter on the impact performance of laminate is analyzed by using a public software package "MINITAB 16". Design of experiments is a powerful analysis tool for modeling and analyzing the influence of control factors on performance output. The most important stage in the design of experiment lies in the selection of the control factors. Exhaustive literature review on impact be-

https://doi.org/10.1017/jmech.2016.24 Published online by Cambridge University Press

havior of polymer composites reveals that parameters *i.e.*, impact velocity, orientation, material of plate, thickness of plate, temperature, volume fraction of SMA and arrangement of SMA *etc*. largely influence the energy absorption of hybrid composites. Three parameters, *i.e.*, temperature, orientation angle and volume fraction of SMA are selected to study their influence using L_{27} orthogonal array of Taguchi in the paper. The operating conditions under which tests carried out are given in Tables 5 and 6.

Table 4 Levels of the variables.

Control factor	Level		
	I	II	III
A: orientation of SMA	0	30	45
B: volume fraction of SMA	60	70	80
C: temperature	50	70	90

Table 5 Results layout using an L_{27} orthogonal array on energy absorption.

Run	Orientation of SMA (A)	Volume fraction of SMA(B)	Temperature (°C)	Energy (J)	S/N ratio (dB)
1	0	60	50	267.6	48.5
2	0	60	70	315.3	50.0
3	0	60	90	365.6	51.3
4	0	70	50	287.5	49.2
5	0	70	70	343.5	50.7
6	0	70	90	402.9	52.1
7	0	80	50	309.9	49.8
8	0	80	70	374.0	51.5
9	0	80	90	442.5	52.9
10	30	60	50	278.8	48.9
11	30	60	70	331.1	50.4
12	30	60	90	387.1	51.8
13	30	70	50	301.7	49.6
14	30	70	70	364.6	51.2
15	30	70	90	432.6	52.7
16	30	80	50	327.9	50.3
17	30	80	70	403.1	52.1
18	30	80	90	485.3	53.7
19	45	60	50	281.7	49.0
20	45	60	70	334.6	50.5
21	45	60	90	391.1	51.8
22	45	70	50	305.0	49.7
23	45	70	70	368.5	51.3
24	45	70	90	437.1	52.8
25	45	80	50	331.4	50.4
26	45	80	70	407.1	52.2
27	45	80	90	489.9	53.8

In Tables 5 and 6, each column represents a test parameter whereas a row stands for a treatment or test condition which is a combination of parameter levels. The result observations are further transformed into signal-to-noise ratio (S/N). The S/N for maximum energy absorption can be expressed as "upper is better" characteristic, which is calculated as logarithmic transformation of loss function shown as below

$$S/N = -10\log\left(\frac{1}{n}\sum_{i=1}^{n}\frac{1}{y_i^2}\right) \tag{22}$$

where "n" the number of observations, and y the observed data.

Table 6 Results layout using an L_{27} orthogonal array on B.P.I.

Run	Orientation of SMA (A)	Volume fraction of SMA (B)	Temperature (°C)	B.P.I.	S/N (dB)
1	0	60	50	31.24	29.89
2	0	60	70	36.81	31.32
3	0	60	90	42.68	32.61
4	0	70	50	31.58	29.99
5	0	70	70	37.72	31.53
6	0	70	90	44.25	32.92
7	0	80	50	32.13	30.14
8	0	80	70	38.78	31.77
9	0	80	90	45.87	33.23
10	30	60	50	32.55	30.25
11	30	60	70	38.66	31.75
12	30	60	90	45.19	33.10
13	30	70	50	33.14	30.41
14	30	70	70	40.05	32.05
15	30	70	90	47.52	33.54
16	30	80	50	34.00	30.63
17	30	80	70	41.79	32.42
18	30	80	90	50.32	34.03
19	45	60	50	32.89	30.34
20	45	60	70	39.07	31.84
21	45	60	90	45.67	33.19
22	45	70	50	33.50	30.50
23	45	70	70	40.47	32.14
24	45	70	90	48.01	33.63
25	45	80	50	34.36	30.72
26	45	80	70	42.21	32.51
27	45	80	90	50.80	34.12

https://doi.org/10.1017/jmech.2016.24 Published online by Cambridge University Press

6. RESULTS AND DISCUSSION

6.1 The Effects of Control Factors on Energy Absorption of Hybrid Composites

The S/N given in Tables 5 and 6 are made using the popular software known as MINITAB 16. The effects of control factors on energy absorption and B.P.I. of hybrid composites are shown in Figs. 3 and 4 respectively. The analysis of the result gives the combination of factors producing maximum energy absorption of the composites. These combinations are found to be different for different hybrid composite materials. The situation combined of A3, B3 and C3 gives maximum energy absorption.

As far as maximization of energy absorbed is concerned, Figs. 3 and 4 reveal that factors C and B have significant effects on all hybrid composites, whereas factor A has least effect. It is observed from Fig. 5 that the interaction between all factors shows insignificant contribution on energy absorption. When B.P.I. is concerned, factor B shows least effect. In addition, A × B and B × C interaction show weak effect on B.P.I. These results are shown in Fig. 6.

The control factors are sorted in relation to the differences in values. The S/N response of the energy absorbed for test specimens is presented in Tables 7 and 8. It is shown that the most effective influence on energy absorbed appeared to be the temperature variations of SMA (factor C), followed by the variation of volume fraction of SMA (factor B) used for the specimens. When B.P.I. is concerned, factor C is still dominant, however, factor B as well as factor C shows low effect.

6.2 ANOVA and the Effects of Factors

In order to find out statistical significance of various factors on the energy absorption, analysis of variance (ANOVA) is performed. It is accomplished by separating the total variability of the S/N, which is measured by sum of the squared deviations from the total mean S/N, into contributions by each of the design parameters and the errors. The p value for each design parameters is calculated. Usually, when $p < 0.05$ it means that the design parameter showed a significant effect.

Tables 9 and 10 show the results of the ANOVA based on the energy absorption and B.P.I. The results indicate the percentage of each factor's contribution on the total variation, exhibiting the degree of influence. It is observed in Table 9 that the temperature has the most significant influence (74.87%) on the energy absorption of hybrid composites, while the volume fraction (21.01%) and orientation (3.61%) are follows. In Table 10, temperature shows the most significant influence (91.57%), the orientation (4.42%) shows the second significant influence and volume fraction (3.39%) is the least significant influence based on the B.P.I. The results also reveal that all interactions between parameters (A × B, A × C and B × C) show least contribution although they have significance (*i.e.* small p-values) in the Tables 9 and 10.

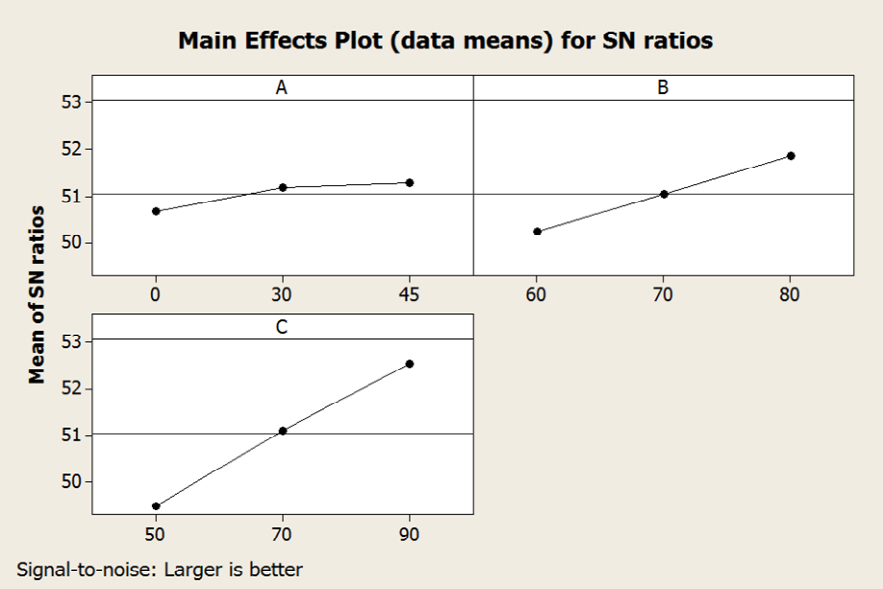


Fig. 3 Effect of control factors on energy absorption of hybrid composites.

https://doi.org/10.1017/jmech.2016.24 Published online by Cambridge University Press

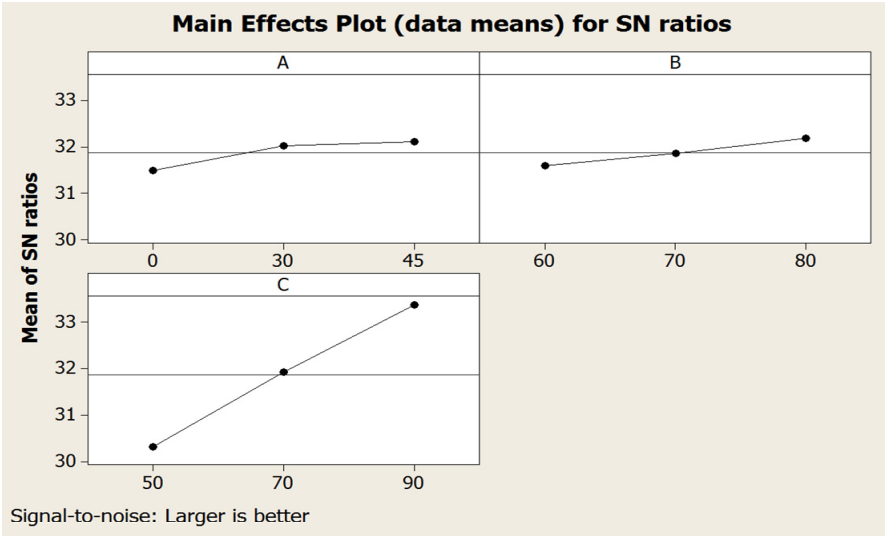


Fig. 4 Effect of control factors on B.P.I. of hybrid composites.

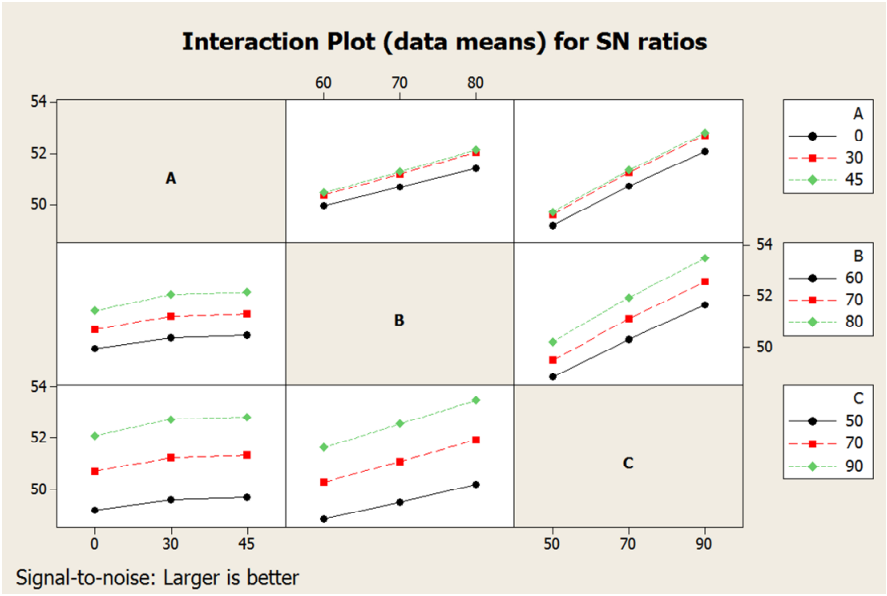


Fig. 5 Interaction graph among A, B, C for energy absorption of hybrid composites.

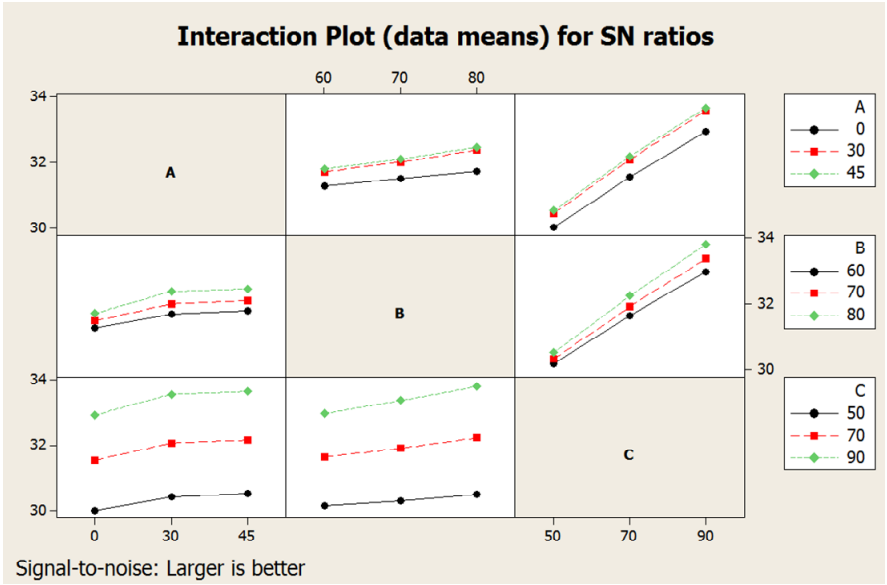


Fig. 6 Interaction graph among A, B, C for B.P.I. of hybrid composites.

https://doi.org/10.1017/jmech.2016.24 Published online by Cambridge University Press

Table 7 Response table of S/N on energy absorption.

Level	A	B	C
1	50.66	50.24	49.49
2	51.19	51.04	51.10
3	51.28	51.86	52.55
Delta	0.62	1.62	3.05
rank	3	2	1

Table 8 Response table of S/N on B.P.I.

Level	A	B	C
1	31.49	31.59	30.32
2	32.02	31.86	31.93
3	32.11	32.17	33.37
Delta	0.62	0.59	3.05
rank	2	3	1

Table 9 Analysis of variance for S/N ratios on energy absorption.

Source	DF	Seq.SS	Adj.SS	Adj.MS	F	P	Contribution (%)
A	2	2.03	2.03	1.01	1650.8	3.660E-11	3.61
B	2	11.79	11.79	5.90	9598.7	3.228E-14	21.01
C	2	42.02	42.02	21.01	34207.2	2.004E-16	74.87
AB	4	0.0487	0.0487	0.0122	19.84	3.478E-04	0.08
AC	4	0.0462	0.0462	0.0116	18.81	4.192E-04	0.08
BC	4	0.1844	0.1844	0.0461	75.05	2.377E-06	0.32
Error	8	0.0049	0.0049	0.0006			0.03
Total	26	56.12					100.00

Table 10 Analysis of variance for S/N ratios on B.P.I.

Source	DF	Seq.SS	Adj.SS	Adj.MS	F	P	Contribution (%)
A	2	2.0278	2.0266	1.0139	1622.24	3.660E-11	4.42
B	2	1.5553	1.5541	0.77765	1244.24	1.055E-10	3.39
C	2	42.019	42.0178	21.0095	33615.20	2.004E-16	91.57
AB	4	0.0487	0.0462	0.012175	19.48	3.478E-04	0.10
AC	4	0.0462	0.0437	0.01155	18.48	4.192E-04	0.10
BC	4	0.1844	0.1819	0.0461	73.76	2.377E-06	0.40
error	8	0.0050	0.0163	0.000625			0.04
Total	26	45.8864	45.8864				100.00

6.3 Confirmation Test

Finally, confirmation test was done to verify the improvement of the quality using the optimal level combination (A3B3C3) of the design parameters for the hybrid composite laminate. The S/N for total energy absorption of the composites can be estimated with the following prediction equation.

$$\eta = \eta_m + \sum_{i=1}^{q} (\eta_i - \eta_m) \tag{23}$$

where η_m is the total mean of the S/N, η_i is the mean of S/N at the optimal level and q is the number of the main design parameters that significantly affect the performance of total energy absorption.

The estimated results, comparing to the initial impact parameters combination (A1B1C1), infer that the S/N is found 5.3dB improvement, corresponding to about 489.9J on total energy absorption. The results are shown as Table 11. In terms of B.P.I., the S/N is found 4.2dB improvement and this corresponding to about 34.12J/m^2, shown as Table 12. The increase of the S/N from initial impact parameters to optimal impact parameters is about 5.3dB, which means that the total energy absorption is increased by about 1.83 times. Regarding the B.P.I., the S/N of optimal impact parameter increases 4.2dB, also about 1.63 times the initial result. Therefore, based on the S/N analysis, the optimal impact parameters for maximum energy absorption of hybrid composites design parameter combinations are temperature (A) at level 3, volume fraction (B) at level 3 and orientation (C) at level 3.

https://doi.org/10.1017/jmech.2016.24 Published online by Cambridge University Press

Table 11 Results of the confirmation tests on energy absorption.

	Initial impact parameters	Optimal impact parameters
Level	A1B1C1	A3B3C3
Energy absorption (J)	267.6	489.9
S/N ratio (dB)	48.5	53.8
Improvement of S/N ratio = 5.3		

Table 12 Results of the confirmation tests on B.P.I.

	Initial impact parameters	Optimal impact parameters
Level	A1B1C1	A3B3C3
B.P.I. (J/m^2)	31.24	50.80
S/N ratio (dB)	29.89	34.12
Improvement of S/N ratio = 4.2		

6.4 Factor Settings for Total Energy Absorption

The relationship among combinations of control factors for total energy absorption of hybrid composites is obtained using linear regression analysis [28-30] model as Eq. (24). SAS 9.3 software was used to determine the coefficients (β_i, i = 0 to 6) of the relation equation. The result is shown as Eq. (25).

$$E = \beta_0 + \beta_1 \times A + \beta_2 \times B + \beta_3 \times C + \beta_4 \times AB + \beta_5 \times AC + \beta_6 \times BC \tag{24}$$

$$E = 203.252 - 1.317 \times A - 0.863 \times B - 096393 \times C + 0.017 \times AB + 0.011 \times AC + 0.055 \times BC \tag{25}$$

$$r^2 = 0.997 \tag{26}$$

The correctness of the determined coefficients is confirmed because high correlation coefficient ($r^2 = 0.997$) greater than 0.95 is obtained and therefore, the model is quite suitable for the further analysis. The objective function to be maximized is given as Eq. (25) for total energy absorption of hybrid composite subjected to constraints as follows:

$$A_{\min} \le A \le A_{\max} \tag{27}$$

$$B_{\min} \le B \le B_{\max} \tag{28}$$

$$C_{\min} \le C \le C_{\max} \tag{29}$$

The suffixes min and max in Eqs. (27) ~ (29) show the lowest and highest control factors settings used in this study (Table 4).

Hybrid Simulated Annealing and Nelder-Mead simplex search algorithm is used to obtain the optimum value of the control factors that maximizes the objective function in this study. Simulated Annealing search algorithm provides a quick and efficient approach to near global optimal design area and Nelder-Mead simplex search is a direct search method for helping approach to the optimum design factor settings. In this paper, computational algorithm of the hybrid optimization search is implemented in MATLAB [31-35].

Table 13 shows the optimum settings of the control factors with the optimum performance output, *i.e.* the maximum energy absorption for hybrid composites.

Table 13 Optimum conditions for performance output.

Orientation of SMA (A)	Volume fraction of SMA (B)	Temperature (C)	Energy (J)
45	80	90	489.9

7. CONCLUSIONS

Based on this work, the following conclusions may be drawn concerning the study of factor settings of shape memory alloy reinforced composite laminates under low velocity impact:

1. Hybrid composites embedded with SMA possess fairly good potential for application in impact. Energy absorption of these composites can be successfully analyzed using laminated plate theory, first-order shear deformation theory, minimal potential energy principle and Taguchi experimental design scheme.
2. The confirmation tests were conducted to verify the optimal impact parameters. The improvement of energy absorption and B.P.I. from the initial to the optimal parameters is about 183% and 163%, respectively.
3. According to ANOVA results, the most significant factor in affecting the energy absorption is temperature (C), with a percentage contribution of 74.87%, followed by volume fraction (B) and orientation (A), with percentage contribution of 21.01% and 3.61%, respectively. However, the most significant factor affecting the B.P.I. is temperature (C), with a percentage contribution of 91.57%, followed by orientation (A) and volume fraction (B), with percentage contribution of 4.42% and 3.39%, respectively. The interactions between the parameters have statistical significance but do not have any physical significance.
4. Optimal factor settings for maximum energy absorption of any hybrid composite can be determined using an effective technique based on hybrid simulated annealing and Nelder-Mead simplex search algorithm adopted in this paper. The hybrid optimization search method is capable of finding a good, feasible, robust, convergent and flexible solution for decision variables and objective function.

https://doi.org/10.1017/jmech.2016.24 Published online by Cambridge University Press

ACKNOWLEDGEMENTS

The authors would like to express their appreciation to Dr. Tien-Chih Liu of the CSIST for his cooperation.

REFERENCES

1. Shokuhfar, A., *et al*., "Analysis and Optimization of Smart Hybrid Composite Plates Subjected to Low-Velocity Impact Using the Response Surface Methodology (RSM)," *Thin-Walled Structures*, **46**, pp. 1204–1212 (2008).
2. John, S. and Hariri, M., "Effect of Shape Memory Alloy Actuation on the Dynamic Response of Polymeric Composite Plates," *Composites Part A: Applied Science and Manufacturing*, **39**, pp. 769–776 (2008).
3. Meo, M., Antonucci, E., Duclaux, P. and Giordano, M., "Finite Element Simulation of Low Velocity Impact on Shape Memory Alloy Composite Plates," *Composite Structures*, **71**, pp. 337–342 (2005).
4. Chen, Y. L., Chen, H. W. and Lin, Y. C., "Analysis of Shape Memory Alloy Hybrid Composite Plates under Low Velocity Impact," *Applied Mechanics and Materials*, pp. 473–476 (2014).
5. Lee, H. J., Lee, J. J. and Huh, J. S., "A Simulation Study on the Thermal Buckling Behavior of Laminated Composite Shells with Embedded Shape Memory Alloy (Sma) Wires," *Composite Structures*, **47**, pp. 463–469 (1999).
6. Chen, Y. L., Chen, H. W. and Lin, Y. C., "A Study of Composite Laminated Plate with Embedded Shape Memory Alloy Wires under Impact Load," *IUMRS-ICEM 2014 International Conference*, Taiwan (2014).
7. Liang, C., and Rogers, C., "One-Dimensional Thermomechanical Constitutive Relations for Shape Memory Materials," *Journal of Intelligent Material Systems and Structures*, **1**, pp. 207–234 (1990).
8. Roh, J.-H. and Kim, J.-H., "Adaptability of Hybrid Smart Composite Plate under Low Velocity Impact," *Composites Part B: Engineering*, **34**, pp. 117–125 (2003).
9. Brinson, L., "One-Dimensional Constitutive Behavior of Shape Memory Alloys: Thermomechanical Derivation with Non-Constant Material Functions and Redefined Martensite Internal Variable," *Journal of Intelligent Material Systems and Structures*, **4**, pp. 229–242 (1993).
10. Brinson, L. and Lammering, R., "Finite Element Analysis of the Behavior of Shape Memory Alloys and Their Applications," *International Journal of Solids and Structures*, **30**, pp. 3261–3280 (1993).
11. Brinson, L., Bekker, A. and Hwang, S., "Deformation of Shape Memory Alloys Due to Thermo-Induced Transformation," *Journal of Intelligent Material Systems and Structures*, **7**, pp. 97–107 (1996).
12. Lee, J. J. and Choi, S., "Thermal Buckling and Postbuckling Analysis of a Laminated Composite Beam with Embedded Sma Actuators," *Composite Structures*, **47**, pp. 695–703 (1999).
13. Auricchio, F. and Sacco, E., "A One-Dimensional Model for Superelastic Shape-Memory Alloys with Different Elastic Properties between Austenite and Martensite," *International Journal of Non-Linear Mechanics*, **32**, pp. 1101–1114 (1997).
14. Wu, Y., Zhong, W., Wu, G. and Zou, J., "Low Velocity Impact Response Analysis of Shape Memory Alloy Reinforced Composite Beam," *Journal of Wuhan University of Technology*, *Materials Science Edition*, **20**, pp. 70–73 (2005).
15. Shariyat, M. and Moradi, M., "Enhanced Algorithm for Nonlinear Impact of Rectangular Compo-site Plates with Sma Wires, Accurately Tracing the Instantaneous and Local Phase Changes," *Composite Structures*, **108**, pp. 834–847 (2014).
16. Shariyat, M., Moradi, M. and Samaee, S., "Enhanced Model for Nonlinear Dynamic Analysis of Rectangular Composite Plates with Embedded Sma Wires, Considering the Instantaneous Local Phase Changes," *Composite Structures*, **109**, pp. 106–118 (2014).
17. Shariyat, M. and Jafari, R., "Nonlinear Low-Velocity Impact Response Analysis of a Radially Preloaded Two-Directional-Functionally Graded Circular Plate: A Refined Contact Stiffness Approach," *Composites Part B: Engineering*, **45**, pp. 981–994 (2013).
18. Birman, V., Chandrashekhara, K. and Sain, S., "An Approach to Optimization of Shape Memory Alloy Hybrid Composite Plates Subjected to Low-Velocity Impact," *Composites Part B: Engineering*, **27**, pp. 439–446 (1996).
19. Wu, Y., Wu, Y., Wang, Y. and Zhong, W., "Study on the Response to Low-Velocity Impact of a Composite Plate Improved by Shape Memory Alloy," *Acta Mechanica Solida Sinica*, **20**, pp. 357–362 (2007).
20. Kim, E.-H., *et al*., "Effects of Shape Memory Alloys on Low Velocity Impact Characteristics of Composite Plate," *Composite Structures*, **93**, pp. 2903–2909 (2011).
21. Mohd Jani, J., Leary, M., Subic, A. and Gibson, M. A., "A Review of Shape Memory Alloy Research, Applications and Opportunities," *Materials and Design*, **56**, pp. 1078–1113 (2014).
22. Ro, J. and Baz, A., "Nitinol-Reinforced Plates: Part Ii. Static and Buckling Characteristics," *Composites Engineering*, **5**, pp. 77–90 (1995).
23. Lu, P., Cui, F. S. and Tan, M. J., "A Theoretical Model for the Bending of a Laminated Beam with Sma Fiber Embedded Layer," *Composite Structures*, **90**, pp. 458–464 (2009).
24. Shiau, L.-C., Kuo, S.-Y. and Chang, S.-Y., "Free Vibration of Buckled Sma Reinforced Composite Laminates," *Composite Structures*, **93**, pp. 2678–2684 (2011).
25. Figucia, F., "Energy Absorption of Kevlar (Trade Name) Fabrics under Ballistic Impact," *DTIC Doc-*

https://doi.org/10.1017/jmech.2016.24 Published online by Cambridge University Press

ument, U.S., pp. 29–41 (1980).
26. Hoo Fatt, M. S., Lin, C., Revilock Jr, D. M. and Hopkins, D. A., "Ballistic Impact of Glare™ Fiber – Metal Laminates," *Composite Structures*, **61**, pp. 73–88 (2003).
27. Hoo Fatt, M. S. and Lin, C., "Perforation of Clamped, Woven E-Glass/Polyester Panels," *Composites Part B: Engineering*, **35**, pp. 359–378 (2004).
28. Mahapatra, S. S. and Patnaik, A., "Study on Mechanical and Erosion Wear Behavior of Hybrid Composites Using Taguchi Experimental Design," *Materials and Design*, **30**, pp. 2791–2801 (2009).
29. Khondker, O. A., Herszberg, I. and Hamada, H., "Measurements and Prediction of the Compression-after-Impact Strength of Glass Knitted Textile Composites," *Composites Part A: Applied Science and Manufacturing*, **35**, pp. 145–157 (2004).
30. Satapathy, B. K., *et al*., "Targeted Material Design of Flyash Filled Composites for Friction Braking Application by Non-Linear Regression Optimization Technique," *Computational Materials Science*, **50**, pp. 3145–3152 (2011).
31. Chang, Y. C., Yeh, L. J. and Chiu, M. C., "Optimization of Constrained Composite Absorbers Using Simulated Annealing," *Applied Acoustics*, **66**, pp. 341–352 (2005).
32. Erdal, O. and Sonmez, F. O., "Optimum Design of Composite Laminates for Maximum Buckling Load Capacity Using Simulated Annealing," *Composite Structures*, **71**, pp. 45–52 (2005).
33. Vasant, P. and Barsoum, N., "Hybrid Pattern Search and Simulated Annealing for Fuzzy Production Planning Problems," *Computers and Mathematics with Applications*, **60**, pp. 1058–1067 (2010).
34. Akbulut, M., and Sonmez, F. O., "Design Optimization of Laminated Composites Using a New Variant of Simulated Annealing," *Computers and Structures*, **89**, pp. 1712–1724 (2011).
35. Li, P., Yang, Y. and Lu, H., "A New Thermal Property Measurement Technique by Modified Pattern Search Method," *Measurement*, **45**, pp. 2121–2127 (2012).

(Manuscript received July 24, 2015,
accepted for publication January 7, 2016.)

https://doi.org/10.1017/jmech.2016.24 Published online by Cambridge University Press